J Biol Inorg Chem (2002) 7: 704–712
DOI 10.1007/s00775-002-0346-2

ORIGINAL ARTICLE

Matteo Dal Peraro · Alejandro J. Vila · Paolo Carloni

Structural determinants and hydrogen-bond network of the mononuclear zinc(II)-β-lactamase active site

Received: 22 August 2001 / Accepted: 14 January 2002 / Published online: 22 March 2002

Abstract Zinc(II)-β-lactamases are among the latest generation of antibiotic-resistant enzymes developed by bacteria against β-lactams. Here we have used density functional theory to provide the full structure of the catalytic site from *Bacillus cereus* mononuclear β-lactamase II. Calculations are carried out on relative large models built on the X-ray structure of the free enzyme at the highest available resolution (1.7 Å, PDB entry **3bc2**). The most stable conformation emerging from our calculations consists of a Zn(II)-bound hydroxide, which acts as nucleophilic agent in the enzymatic reaction, highly stabilized by a complex hydrogen-bond network, in which the protonation state of Asp90 plays a major role. The pattern differs from that previously proposed on the basis of smaller models. Furthermore, the calculations confirm that Arg91 contributes to determine the orientation and the protonation state of Asp90, as recently suggested by mutagenesis experiments. Electronic supplementary material to this paper, comprising two tables and three figures, can be obtained by using the Springer Link server located at http://dx.doi.org/10.1007/s00775-002-0346-2.

Keywords Mononuclear zinc(II)-β-lactamase · *Bacillus cereus* β-lactamase II · Hydrogen-bond network · Protonation state · Density functional theory geometry optimization

Electronic supplementary material to this paper, comprising two tables and three figures, can be obtained by using the Springer Link server located at http://dx.doi.org/10.1007/s00775-002-0346-2

M. Dal Peraro · P. Carloni (✉)
International School for Advanced Studies,
S.I.S.S.A., via Beirut 2-4, 34014 Trieste, Italy
E-mail: carloni@sissa.it
Tel.: +39-040-3787407
Fax: +39-040-3787528

M. Dal Peraro · P. Carloni
Istituto Nazionale di Fisica della Materia,
INFM, Sezione di Trieste, Italy

A.J. Vila
Biophysics Section and Istituto de Biologia Molecular y Celular de Rosario (IBR), University of Rosario,
Suipacha 531, S2002LRK Rosario, Argentina

Introduction

β-Lactamases (E.C. 3.5.2.6) stand as the major resistance mechanism developed by bacteria against the action of β-lactam antibiotics. These enzymes catalyze the hydrolysis of the four-membered β-lactam ring present in these drugs, rendering them ineffective against their targets [1, 2].

β-Lactamases have been classified into four classes according to sequence homology (A-D) [3]. Enzymes from classes A, C and D use a serine residue to perform the nucleophilic attack at the carbonyl group of the lactam moiety (“serine-β-lactamases”). Several studies on these enzymes have led to the design of potent drugs which efficiently thwart their action [4]. In contrast, no clinically useful inhibitors have yet been identified against the latest generation of β-lactamases, the class B enzymes or metallo-β-lactamases. These proteins, which are characterized by one or two Zn(II) ions at the active site, use a metal-bound water or hydroxy group as the nucleophilic agent [5, 6, 7, 8].

Sequence and structural similarity within the family of class B enzymes suggests a prima facie that they may share a common catalytic mechanism. Notwithstanding, metallo-β-lactamases from different sources exhibit a remarkable catalytic diversity. The different requirements of metal ion content in different organisms represent the most outstanding example of this diversity. The enzymes CcrA from *Bacteroides fragilis* [9, 10], L1 from *Stenotrophomonas maltophilia* [11] and the plasmidic enzyme IMP-1 [12] are fully active with two tightly bound Zn(II) ions in the active site. On the other hand, the enzymes β-lactamase II from *Bacillus cereus* (βLII hereafter) [13, 14] and CphA from *Aeromonas hydrophila* are active with one Zn(II) ion per enzyme [15]. Uptake of a second Zn(II) equivalent slightly enhances the activity of the *B. cereus* enzyme [13], whereas

in the *A. hydrophila* β-lactamase exerts an inhibitory effect [16]. This evidence suggests that metallo-β-lactamases share a zinc binding motif, whose features may be notably regulated by the protein milieu.

Studies aimed at the investigation of the catalytic mechanism of these enzymes, or at computer-aided drug design, rely on knowledge of the protonation state of the residues in the active site, including the Zn(II)-bound water/hydroxide moiety that is supposed to be active as the nucleophile in catalysis [5].

A considerable wealth of structural [8, 9, 12, 17, 18], biochemical [14, 19] and mechanistic [10, 20, 21, 22] information has recently become available for both the binuclear and mononuclear enzymes. Based on this information, ab initio calculations have provided the description of plausible protomers of the active sites, both in mono- [23, 24] and binuclear conformations [25]. However, the absence of groups which play a fundamental role for the catalysis may affect the energetics of the systems.

Here we have addressed this issue by performing density functional theory calculations on the mono-Zn(II) lactamases from *B. cereus*. In contrast with previous studies [24], we include, besides the His_3Wat coordination Zn(II) shell, all of the residues which are known to be catalytically relevant: (1) Asp90, anchoring the nucleophilic agent [7]; (2) His210, already proposed in previous simulations as a proton donor assistant in the reaction [23, 24]; (3) Cys168, H-bonded to a water/hydroxy group [7]; and finally (4) Arg91, that has been recently proposed, on the basis of site-directed mutagenesis experiments, as involved in catalytic arrangement of the active site [26]. Our calculations, which are based on a high-resolution structure (1.7 Å, PDB entry **3bc2**, Fig. 1), suggest that the Zn(II)-bound hydroxide is the catalytically active nucleophile, providing a strong H-bond pattern for the active site that accounts for the presence of some conserved residues in these enzymes. Furthermore, our findings confirm the important role of Arg91, as evidenced on the basis of mutagenesis data [26]. Our findings provide a different description of the H-bond pattern than that proposed based on models including only the Zn(II) coordination sphere, Asp90 and His210 [23, 24]. Thus, inclusion of Cys168 and mainly of Arg91 surrounding groups appears of fundamental importance to thoroughly describe the biological and structural determinants of the enzyme.

Methods

Structural models

Several crystal structures of the mono-Zn(II) form of *B. cereus* βLII enzyme are available[1]. The earliest was solved at 2.5 Å resolution (PDB entry **1bmc** [8]); it features a Zn(II) ion adopting a tetrahedral geometry, coordinated to three His residues and a water/hydroxide molecule, located beyond bonding distance (3.3 Å). The structure of the Cys168→Ser mutant has been solved at 1.85 Å resolution (PDB entry **1dxk** [27]). It indicates that the H-bond pattern is altered upon mutation of the Cys residue. The structures at the highest resolution (1.7 Å, PDB entries **2bc2** and **3bc2**) show that the Zn(II) displays a regular His_3Wat four-coordinated geometry (Fig. 1). In these structures, Cys168 is oxidized, thus partly altering the H-bond architecture in the active site. We chose one of these structures, namely **3bc2**, in which His210 appears to have the correct orientation so as to interact with Asp90 (Fig. 1), as proposed previously [23, 24]. On the other hand, the active site of **2bc2** presents a structural rearrangement which appears to be in contrast to previous suggestions [23, 24]. In particular, the His210 side chain flips out from the active site (see Supplementary material, Fig. S1).

The models include (1) the catalytic Zn(II) ion (Zn in Fig. 1); (2) the Zn(II) coordination sphere, composed of His86, His88, His149 and a water or hydroxide molecule (OW); (3) Asp90; (4) Cys168, whose sulfur-bonded oxygens were removed; (5) His210, which H-bonds to Asp90; and (6) Arg91, which is oriented towards Cys168 in the crystal structure, owing to the oxidation state of the Cys residue (Fig. 1). The residues considered were truncated at the β-carbon atom, following the suggestions of Carloni et al. [28]; His was modeled as 4- or 5-methylimidazole, Asp as acetate, Cys as methanethiol and Arg as $[CH_3CH_2\text{-}NH\text{-}C(NH_2)_2]^+$.

The protonation state of Asp90, His210 and OW is uncertain. Thus, several plausible protomers were considered[2]. For the other residues in the active site (His86, His88, His149 and Cys168), the protonation state appears to be obvious (Fig. 2). During geometry optimization, in model **E** the Zn(II)-bound water transfers spontaneously a proton to Asp90, giving rise to model **B**; furthermore, in model **F**, Asp90 transfers a proton to OW, providing model **D**. Thus, only four different protomers were studied (**A-D**, Fig. 2).

Similar protomers (**A-D**) were built based on the low-resolution structure **1bmc**, obtained in non-oxidative conditions [8]. The active site of this structure differs from **3bc2** by the orientation of Arg91, strongly H-bonded to Asp90, and by the location of the Zn(II)-bound water/hydroxide, being beyond bonding distance from the metal ion (3.3 Å). The overall RMSD between two crystals is, however, very small (0.5 Å, see Supplementary material, Table S1 and Fig. S2).

Quantum chemistry

Ab initio calculations were performed in the framework of density functional theory (DFT) using the Car-Parrinello [29] program CPMD 3.4 [30]. We adopted the BLYP generalized gradient approximation exchange-correlation functional [31, 32], which has been shown to describe accurately the structure and bonding of a variety of other enzymatic systems [33].

The valence shell electrons were described by a plane wave basis set up to an energy cutoff of 70 Ry. The interaction between valence shell and core electrons was described by a norm-conserving pseudopotential of the Troullier-Martins type [34]; the method of Kleinman and Bylander [35] [Gauss-Hermit for Zn(II) ion] was used for the calculation of the non-local parts. This setup has been shown to accurately describe the Zn(II) sites in the enzymes carbonic anhydrase [36] and alcohol dehydrogenase [37].

The models were inserted in an orthorhombic box of $15\times17\times18$ Å^3. They were treated as isolated systems using the method of Martyna and Tuckerman [38]. No constraints were applied. The method of direct inversion in the iterative subspace [39] was used for the optimizations of the ionic positions, to reach a standard convergence of 5×10^{-4} (the maximum value for the largest element of the gradient). A single optimization timestep employed about 40 s of CPU time on a 16-processor IBM SP3 parallel machine.

[1]Table S1 in the Supplementary material compares the RMSD values of each active site structure with respect to the others

[2]Protomers in which the water molecule OW and Asp90 are protonated were not considered because they exhibit an excessively large positive charge in the metal active site (Fig. 2)

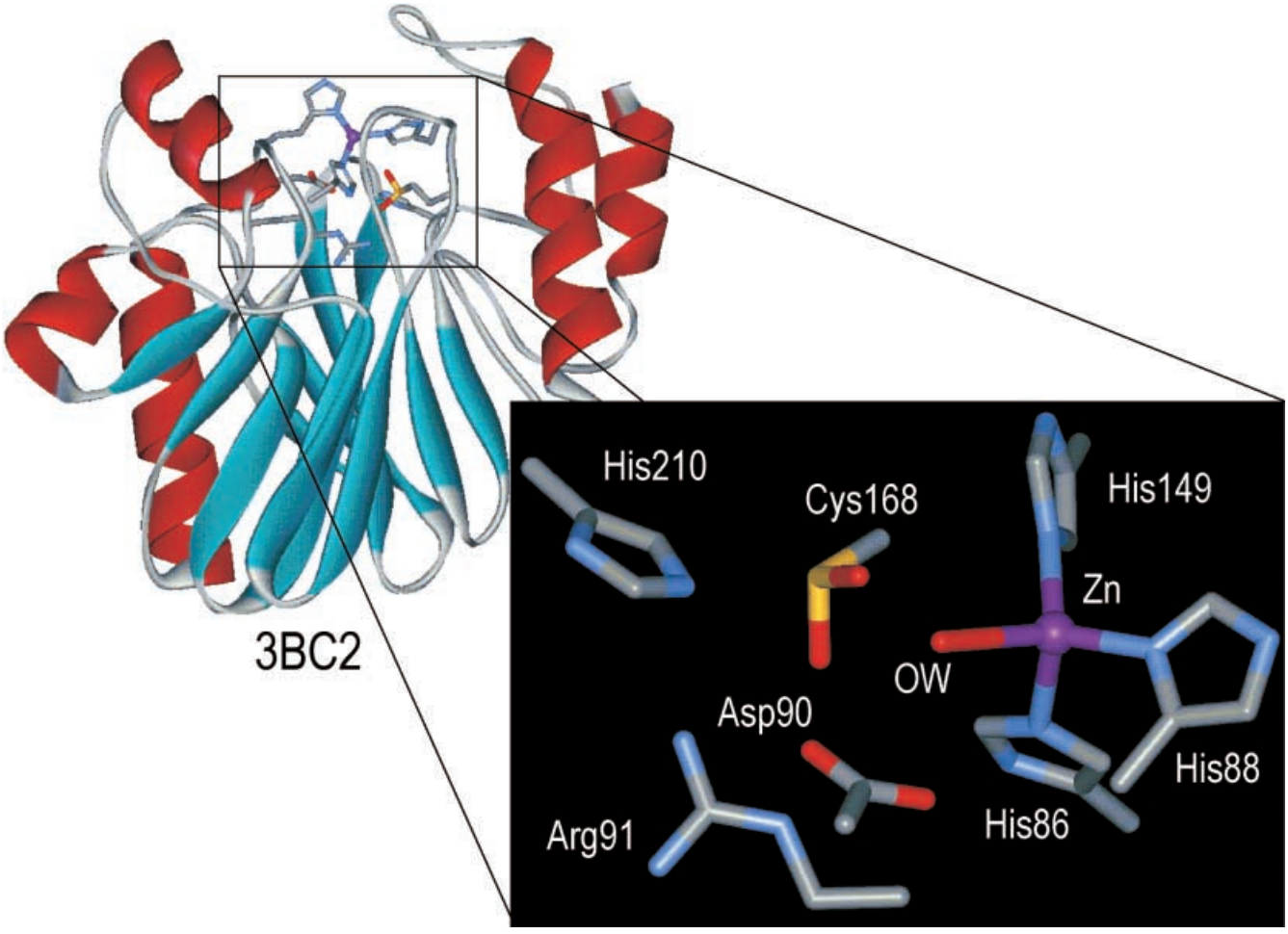

Fig. 1. Structure of Zn(II)-β-lactamase from *B. cereus* (**3bc2**). Overall folding and active site are represented as *ribbons* and *ball-and-sticks*, respectively. The close-up focuses on the active-site structure. The Zn(II) is tetrahedrally coordinated by His86, His88, His149 and a water/hydroxide molecule. The H-bond network involved in the OW nucleophile orientation includes the conserved residues Asp90, Cys168 and His210, that also act as metal ligands of the second Zn(II) ion in binuclear β-lactamases. Cys168 is oxidized in this structure and interacts with OW and Arg91; the latter is highly conserved in mononuclear enzymes and engaged in the H-bond network, as suggested by recent mutagenesis experiments [26]

Energy calculations

Comparison of the energetics of different protomers is not straightforward owing to their different proton content. To correct the energies we have added to models **B**, **C** and **D** a term which takes into account the energy loss due to dehydration of a proton from the water environment [hydration enthalpy, $\Delta E(H^+)$]. Within DFT, this term was calculated as:

1. The energy obtained by inserting an H^+ in a cluster of n water molecules $(H_2O)_n$ (n from 1 to 7[3]):

$$H^+ + (H_2O)_n \rightarrow \left[(H_2O)_{n-1}{-}H_3O\right]^+ \quad (1)$$

2. The energy obtained to form the $[(H_2O)_{n-1}{-}H_3O]^+$ complex from a proton and n isolated water molecules:

$$H^+ + nH_2O \rightarrow \left[(H_2O)_{n-1}{-}H_3O\right]^+ \quad (2)$$

Both calculations provided $\Delta E(H^+) \approx 250$ kcal/mol: an inferior limit estimation of $\Delta E(H^+)$ in fair agreement with the experimental data (263 kcal/mol [40][4]).

Calculated properties

The charge distribution was calculated with the ESP partial atomic charges [41]. Changes in chemical bonding on passing from one complex to another were monitored in terms of rearrangement of the *maxima* of the Boys' orbitals [42, 43, 44]. Polarization effects were estimated in terms of the electronic density difference between the entire system and its n constituents: $\Delta\rho = \Delta\rho_{tot} - \Sigma^n{}_{i=1}\Delta\rho_i$.

Results

Bonding, structures and energetics of the protomers in Fig. 2, based on the high-resolution structure **3bc2**, are presented in Tables 1, 2, 3[5], respectively. These

[3]Calculations on clusters with more than seven waters were not carried out because of their computational cost. No attempts were made to calculate entropy effects

[4]Further details are available in the Supplementary material, Fig. S3)

[5]The geometry optimized structures of models **E** and **F** turn out to be identical to **B** and **D**, respectively (see Methods section). These models are not considered here

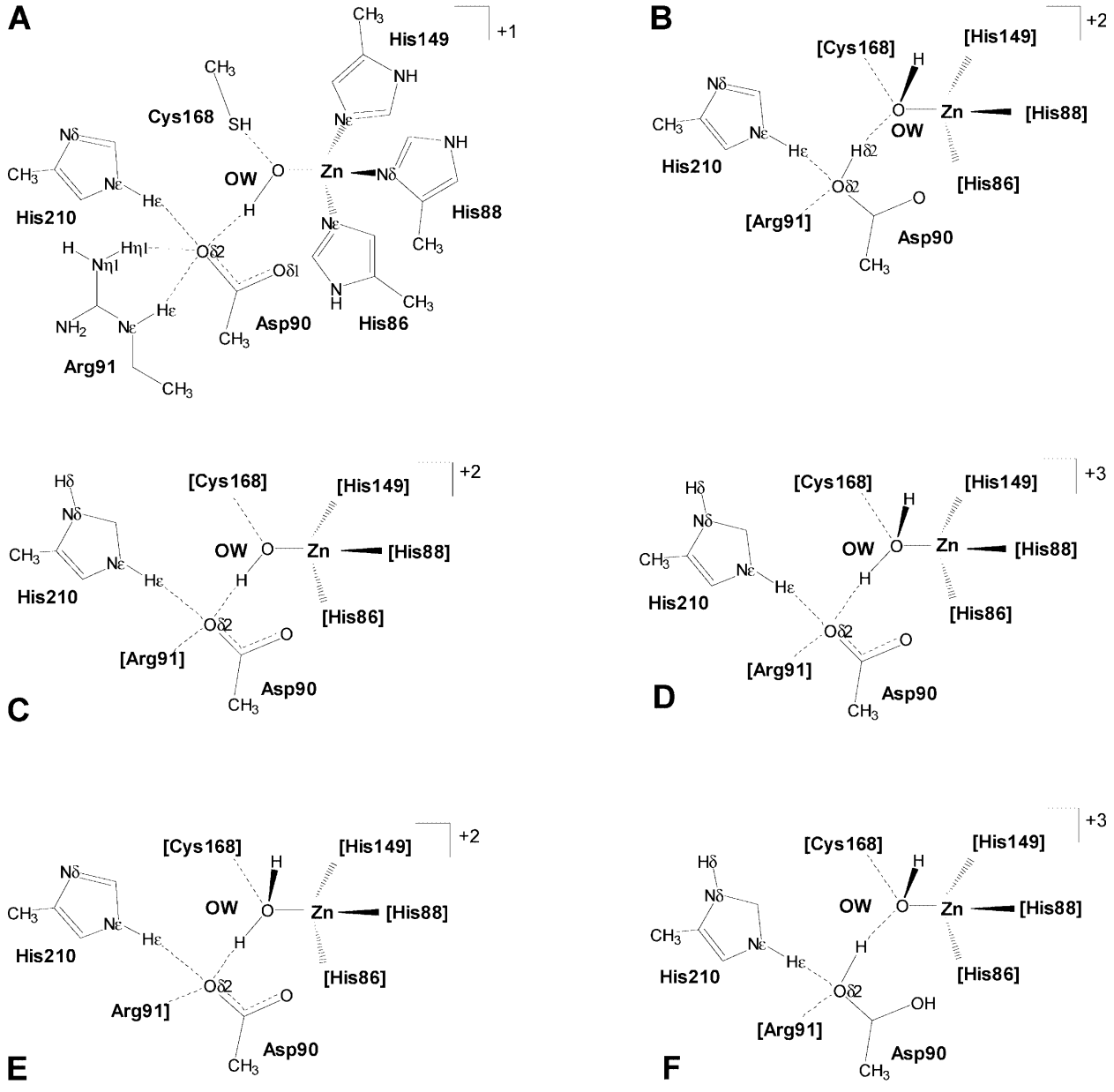

Fig. 2A–F. Possible protomer models

protomers differ by the protonation states of Asp90, His210 and OW (see Figs. 2 and 3). The optimized geometries of the four models turned out to be very similar to that of the X-ray structure (Fig. 3), the RMSDs ranging from 1.7 to 1.8 Å (see Supplementary material, Table S2). The largest structural rearrangements during optimization involve OW and Arg91, which interact with the oxidized form of Cys168 in the X-ray structure (Fig. 1). These interactions are absent as we have used the reduced models. As a result, Arg91, by rotating its guanidinium plane by about 60°, forms a salt bridge with Asp90. OW, however, moves closer to Cys168, shortening the O@OW-Zn(II) bond distance with respect to X-ray structure, and distorting the original Zn(II) coordination polyhedron, more irregular in optimized structures (Table 2).

Table 1. H-bonds network. Selected H-bond distances (in Å) of models **A** and **B**, compared to X-ray reference structure. Atom names are the same as Fig. 2

	A	**B**	**3bc2**
Oδ2@Asp90-H@OW	2.13	–	–
Oδ2@Asp90-O@OW	3.07	2.55	3.02
Hδ2@Asp90-O@OW	–	1.49	–
Oδ2@Asp90-Hϵ@His210	2.30	2.62	–
Oδ2@Asp90-Nϵ@His210	3.24	3.57	3.72
Oδ2@Asp90-Hη1@Arg91	1.76	2.25	–
Oδ2@Asp90-Nη1@Arg91	2.85	3.15	4.02
Oδ2@Asp90-Hϵ@Arg91	1.93	2.11	–
Oδ2@Asp90-Nϵ@Arg91	2.72	3.07	3.37
H@Cys168-O@OW	1.85	2.78	–
S@Cys168-O@OW	3.23	4.00	4.14

Table 2. Zn(II) coordination polyhedron. Comparison between calculated and experimental structural parameters. Distances (*d*) are in Å and the angles (∠) in degrees. Atoms names are the same as Fig. 2

	A	B	C	D	3bc2
***d*[Zn-Nϵ@His86]**	2.15	2.10	2.07	2.07	2.28
***d*[Zn-Nδ@His88]**	2.09	2.06	2.07	2.05	1.95
***d*[Zn-Nϵ@His149]**	2.18	2.17	2.10	2.08	2.11
***d*[Zn-O@OW]**	1.90	1.96	1.98	2.03	2.50
∠[Nϵ@His86-Zn-Nδ@His88]	101	106	105	108	105
∠[Nδ@His88-Zn-Nϵ@His149]	102	106	108	113	112
∠[Nϵ@His149-Zn-O@OW]	98	104	104	105	109
∠[O@OW-Zn-Nϵ@His86]	112	108	110	106	104

Table 3. Energetics. Absolute and relative energies (in kcal/mol) of models **A–D**; **A** and **B** are considered also in the absence of Arg91. The energies have been corrected following the procedure outlined in the Methods section (see also Fig. S3 in the Supplementary material)

	A	B	C	D	A – Arg91	B – Arg91
***E*(i)**	–234,584.6	–2345,40.7	–234,543.2	–234,459.1	–201,596.9	–201,622.0
Δ*E*	0.0	43.9	41.4	125.5	0.0	–25.1
***E*(ii)**	–234,584.6	–234,553.2	–234,555.7	–234,471.6	–201,596.9	–201,634.6
Δ*E*	0.0	31.4	28.9	113.0	0.0	–37.7

Model **A**, in which His210 is neutral and Asp90 deprotonated (Fig. 2), is characterized by a strong H-bond network: Asp90 tightly H-bonds the Zn(II)-bound hydroxide OW, Arg91 and His210 (Fig. 3A and Table 1), and Cys168 is H-bonded to OW. The Zn(II) coordination is a distorted tetrahedral polyhedron (Table 2). Only OW deviates from the ideal geometry, presumably because of its strong H-bond interactions with Asp90 and Cys168 (Fig. 3A).

Model **B** assumes His210 and Asp90 as neutral, and gives rise to a minimized structure less stable than **A** by several tens of kcal/mol (∼30/40 kcal/mol, see Table 3). This might be ascribed to changes in the H-bond pattern. Indeed, Asp90, which acts as an *H-bond donor* to OW, induces a reorientation of the hydrogen atom of OW. This causes the loss of the OW-Cys168 interaction (Fig. 3B, Table 1). Moreover, in this model also the Asp90-His210 H-bond is lost.

Finally, models **C** and **D**, in which His210 is protonated, turned out to be even higher in energy (see Table 3). The relative high energy of the complexes is presumably due to the unlikely protonation pattern that mainly perturbs the displacement of Asp90; this residue approaches, owing to electrostatic interaction, His210, moving its axis off about 1 Å with respect to the crystal reference (Fig. 3C, D). In sum, the presence of positively charge His210, in competition with Arg91, provides an unfavorable electrostatic stabilization of the active site and a disruption of Asp90 orientation.

Calculations based on the low-resolution non-oxidized structure (**1bmc**) provided *identical* structural optimized models. In particular, during these optimizations the metal-bound OW, which is located far from the Zn(II) ion in the X-ray structure (3.3 Å) [45], moves towards the Zn(II) ion until reaching a regular bonding distance. As in the case of **3bc2**, the RMSDs between the **A–D** optimized structures and the initial X-ray structure assume similar values, ranging from 1.4 to 1.8 Å (see Supplementary material, Table S2).

Two different calculations allow us therefore to conclude that a hydroxide molecule binds the Zn(II) ion and that model **A** is the most stable protomer representing the mononuclear enzyme active site.

The last step of our investigation focuses on Arg91, an important residue for the enzymatic function in mono-Zn(II) βLII [26]. To explore the role of Arg91 for the structural properties at the active site, we removed this residue in the **A** and **B** models. Both optimized structures (models **A** minus **Arg91** and **B** minus **Arg91**) present conformational differences with respect to the X-ray structure and previous optimized models; specifically, Asp90 is more distorted when deprotonated (model **A**), maybe due to the disruption of a salt bridge with the guanidinum group of Arg91 (Fig. 4A).

Removal of Arg91 has consequences also on the *energetics* and the *electronic properties*: **B** minus **Arg91** (or protomer with Asp90 protonated) becomes energetically more stable than **A** minus **Arg91** (Table 3); furthermore, in both models the ESP partial atomic charges [41] of the model's metal ion[6] are significantly less positive (Table 4). In addition, the *maxima* of the Boys' orbitals [42, 43, 44] of the Asp90 carboxy group, which can be associated with the oxygen lone pairs and with the C-O bond, change significantly for **A** minus **Arg91** (up to 0.06–0.07 Å) but less relevantly for **B** minus **Arg91** (0.02 Å). Finally, as depicted in Fig. 5, Arg91 strongly polarizes Asp90 in model **A**, while the relevance of this polarization seems to be less prominent in **B** (Fig. 5B).

[6]The ESP charges analysis revealed a significant difference in the charge distribution between **A** and **B** (Table 4): the Zn(II) ion loses half of its charge in B because of the presence of an added proton with respect to the **A** model

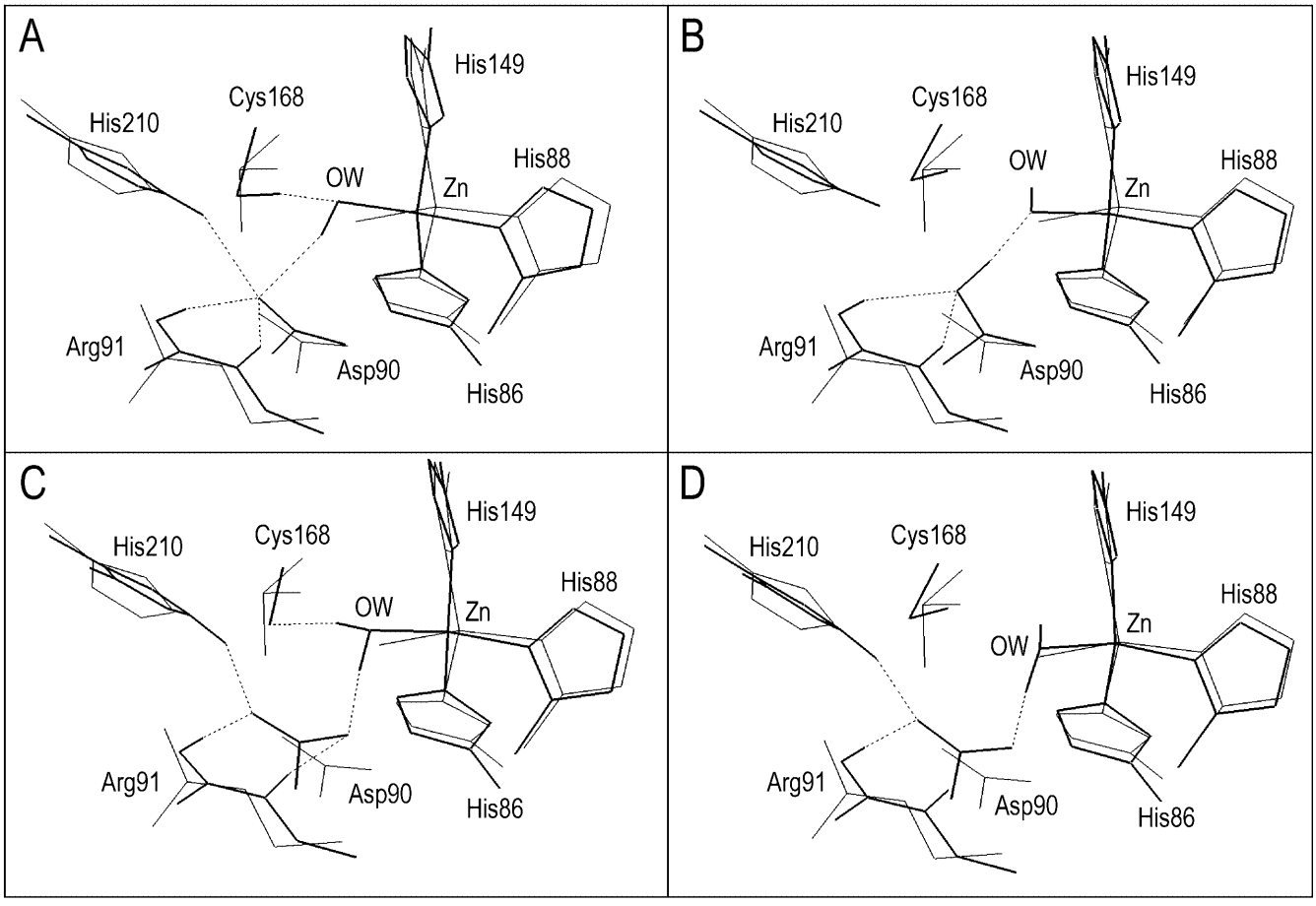

Fig. 3A–D. Geometry optimized models. The structures are schematically represented by *thick lines*; the 3bc2 X-ray structure is also displayed in *thin lines* (relative RMSD values are reported in the Supplementary material, Table S2). For sake of clarity, the picture shows only the hydrogen atoms forming H-bond interactions (represented as *dashed lines*)

We therefore conclude that residue Arg91 contributes to delineate the structural, energetic and electronic properties of the active site as represented by model **A**.

Discussion

In the present study, we have used first principle quantum chemical calculations to establish the protonation

Fig. 4A, B. Arg91 structural role. Optimized models **A** and **B** (in *thin lines*) are superimposed onto models without Arg91 (A – Arg91 and B – Arg91). For sake of clarity, the picture shows only the hydrogen atoms forming H-bond interactions (represented as *dashed lines*)

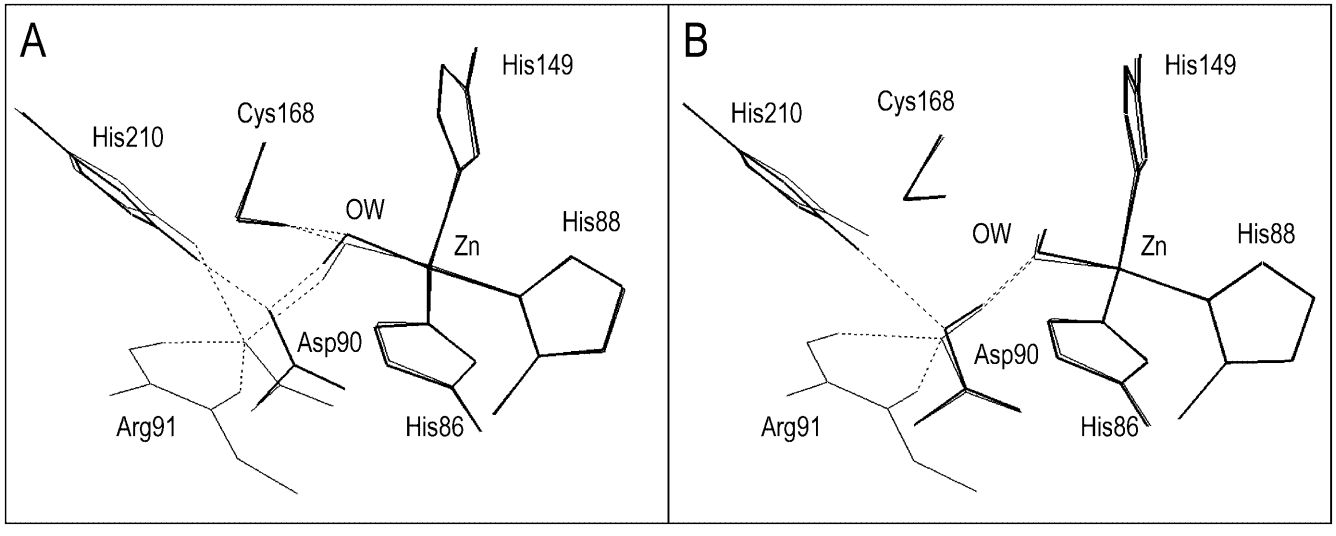

Table 4. ESP charges [41] of selected atoms in models **A** and **B**, with and without Arg91. Atom names are the same as Fig. 2

	A	B	A – Arg91	B – Arg91
Zn	0.30	0.18	0.15	0.09
O@OW	–1.07	–0.71	–1.03	–0.62
H@OW	0.43	0.26	0.48	0.24
Oδ2@Asp90	–0.48	–0.57	–0.78	–0.73
Hδ2@Asp90	–	0.44	–	0.47
Nϵ@His86	0.16	0.34	0.19	0.24
Nδ@His88	0.24	0.31	0.18	0.20
Nϵ@His149	0.13	0.13	0.06	0.02
H@Cys168	0.37	0.09	0.40	0.08
S@Cys168	–0.42	–0.26	–0.19	–0.12

state of the Zn(II) active site in the enzyme βLII from *B. cereus*, based on the highest resolution structure. The calculations provide evidence that model **A** is the most stable protomer: it is more stable than the other models by at least 30 kcal/mol (Table 3). The structural model produced in this research, which is available on the web at the address http://www.sissa.it/cm/bc/, may be used to dock inhibitors and to investigate the reaction mechanism.

The structural features of the groups forming the active site are discussed below, and then compared with those of the binuclear β-lactamases.

Zn(II) coordination polyhedron

Our calculations suggest that a hydroxide molecule binds the Zn(II) ion. The presence of an OH^- ion bound to the metal ion was suggested previously [5, 6, 7, 8]. The calculated Zn(II)-O bond distances (Table 2) are consistent with the high-resolution structures of β-lactamases and other Zn(II)-hydroxide species (e.g. the carbonic anhydrase enzyme) and they agree well with Zn(II)-O distances experimentally observed in the structures of binuclear β-lactamases [9, 12]. Also the structural parameters of the other Zn(II) ligands, such as N@His-Zn(II) distances, are well maintained in the optimized structure (Table 2).

His210

Our findings contrast with previous ab initio calculations performed on smaller models, which suggest that His210 is protonated [24]. In that study, the positively charged residue is suggested to mediate the hydrolysis reaction of β-lactams by a proton transfer, through Asp90, on the nucleophilic hydroxide [24]. However, here we find that the presence of a positively charged residue perturbs greatly the electrostatic stability of the metal site: His210 strongly attracts Asp90, in competition with the Arg91-Asp90 salt bridge. This results in a structural rearrangement of Asp90, maybe not functionally optimally oriented for catalysis assistance. A neutral His210, acting as *H-bond donor* to Asp90, describes better the structural determinants of the active site, preserving the electrostatic interactions between the Zn(II)-OW-Asp90-Arg91 bridge.

Asp90

The deprotonated Asp90 in model **A**, by acting as an *H-bond acceptor*, forms a strong H-bond interaction with OW and a stable salt bridge with the Arg91 guanidinum group (Fig. 3A and Table 1). The Zn(II)-bound hydroxide in turn acts as an H-bond acceptor of the Cys168 thiol group. The presence of deprotonated Asp90 as aspartate is consistent with the mechanism proposed by Bounaga et al. [5] and Lim et al. [46], which required this group to be deprotonated. Based on our

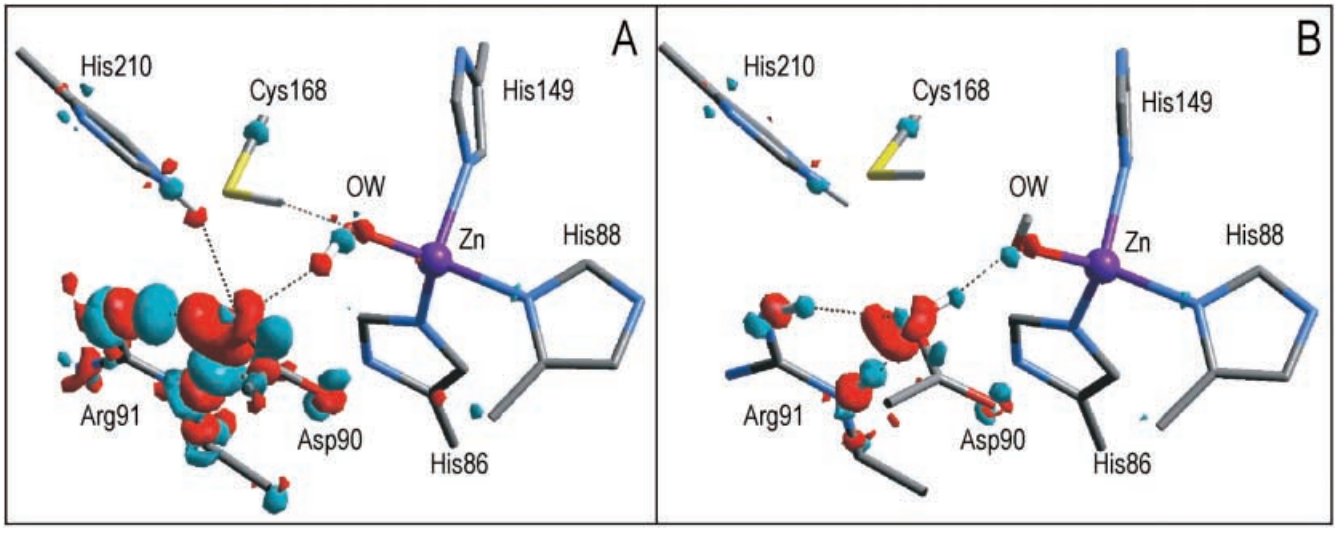

Fig. 5A, B. Polarization effects of Arg91. Plot of the electron density difference, $\Delta\rho = \Delta\rho_{tot} - \Delta\rho_{tot-Arg91} - \Delta\rho_{Arg91}$, superimposed on models A and B (in *cylinders* representation); positive (negative) isodensity surfaces (0.03 a.u.) are drawn in *red* (*light blue*). For sake of clarity, the picture shows only the hydrogen atoms forming H-bond interactions (represented as *dashed lines*)

results, here we propose that a deprotonated Asp90 may be also needed to properly orient the Zn(II)-bound OW for nucleophilic attack at the β-lactam ring. Indeed, substrate docking on models **A** and **B** (that will be reported elsewhere) suggests that in the deprotonated species the hydroxide group OW approaches parallel to the O=C bond of the β-lactam ring, with one of the oxygen lone pairs oriented towards the carbon atom, similar to what has been found for carbonic anhydrase [47]. In contrast, if Asp90 is protonated (model **B**), not only the orientation of the lone pairs is not adequate for nucleophilic attack, but the orientation of the hydroxide sterically hinders substrate binding.

Arg91

Our calculations provide evidence that this residue is important for the structure and energetics of the active site. Indeed, Arg91 is involved in a strong H-bond interaction with Asp90 and its removal (model **A** minus **Arg91**, Fig. 4A) has major consequences.

Comparison between the **A** and **A** minus **Arg91** structures (Fig. 4A) shows that the highly favorable Asp90-Arg91 electrostatic interaction provides a relevant stabilization effect for the Zn(II)-OW-Asp90-Arg91 moiety (Fig. 5), contributing to the exact orientation of OW for nucleophilic attack. The structural changes are reflected in variations of the electronic structure (for instance, the ESP [41] partial charge of Zn(II) ion halves, Table 4) and on the energetics: the deprotonated form, **A** minus **Arg91**, is less stable than **B** minus **Arg91** (Table 3). These findings are consistent with the fact that Arg91 is exclusively conserved in mononuclear β-lactamases [6]; furthermore, they may offer an explanation for the drop in the k_{cat} value of the mononuclear species upon the Arg91→Cys mutation [26], as the optimal orientation of hydroxide OW may be lost in the mutated enzyme.

Comparison with the binuclear enzyme

These results highlight the relevance of Arg91 in the catalytic mechanism. We propose here that Arg and the second Zn(II) could play equivalent roles in the enzymatic reaction in mono- and binuclear enzymes, respectively. Indeed (1) Arg91 anchors the Asp90 side chain by forming a strong H-bond, ultimately orienting the the Zn(II)-bound hydroxide for nucleophilic attack at the antibiotic β-lactam ring; (2) Asp90, Cys168 and His210 are involved in the H-bond network at the active site. In mononuclear enzymes, these residues (together with Arg91) might contribute to nucleophile orientation and stabilization of a Zn(II)-bound hydroxide (with respect to a water molecule). Instead, in binuclear enzymes, the Asp90-Cys168-His210 triad would provide a zinc binding motif. The second Zn(II) ion, by simultaneously binding OW and Asp90, would fulfill the anchoring role and the hydroxide stabilization. Hence, Arg91 would be no longer needed. This picture suggests that these residues may be modularly exploited in different ways by metallo-β-lactamases, according to the zinc content.

Acknowledgements We would like to thank the anonymous referees for their suggestions. A.J.V. acknowledges financial support from Agencia Nacional de Promoción Científica y Tecnológica (PICT 99-01-6616), CONICET (PIP 0582/99), and an early career grant from Fundación Antorchas. A.J.V. is a staff member from CONICET, an International Research Scholar of the HHMI, and a Carrillo-Oñativia Fellow from the Ministry of Health (Argentina). R.M. Rasia is acknowledged for helpful discussions. Financial support of the INFM is also greatly acknowledged.

References

1. Frere JM (1995) Mol Microbiol 16:385–395
2. Bush K, Jacoby GA, Medeiros AA (1995) Antimicrob Agents Chemother 39:1211–1233
3. Ambler RP (1980) Philos Trans R Soc Lond Ser B 289:321–331
4. Di Modugno E, Felici A (1999) Curr Opin Anti-infect Invest Drugs 1:26–42
5. Bounaga S, Laws AP, Galleni M, Page MI (1998) Biochem J 331:703–711
6. Cricco JA, Vila AJ (1999) Curr Pharm Des 5:915–927
7. Cricco JA, Orellano EG, Rasia RM, Ceccarelli EA, Vila AJ (1999) Coord Chem Rev 190–192:519–535
8. Wang Z, Fast W, Valentine AM, Benkovic SJ (1999) Curr Opin Chem Biol 3:614–622
9. Concha NO, Rasmussen BA, Bush K, Herzberg O (1996) Structure 4:823–836
10. Wang Z, Fast W, Benkovic SJ (1999) Biochemistry 38:10013–10023
11. Ullah JH, Walsh TR, Taylor IA, Emery DC, Verma CS, Gamblin SJ, Spencer J (1998) J Mol Biol 284:125–136
12. Concha NO, Janson CA, Rowling P, Pearson S, Cheever CA, Clarke BP, Lewis C, Galleni M, Frere JM, Payne DJ, Bateson JH, Abdel-Meguid SS (2000) Biochemistry 39:4288–4298
13. Orellano EG, Girardini JE, Cricco JA, Ceccarelli EA, Vila AJ (1998) Biochemistry 37:10173–10180
14. Paul-Soto R, Hernandez-Valladares M, Galleni M, Bauer R, Zeppezauer M, Frere JM, Adolph HW (1998) FEBS Lett 438:137–140
15. Hernandez VM, Felici A, Weber G, Adolph HW, Zeppezauer M, Rossolini GM, Amicosante G, Frere JM, Galleni M (1997) Biochemistry 36:11534–11541
16. Hernandez Valladares M, Kiefer M, Heinz U, Soto RP, Meyer-Klaucke W, Nolting MF, Zeppezauer M, Galleni M, Frere JM, Rossolini GM, Amicosante G, Adolph HW (2000) FEBS Lett 467:221–225
17. Fabiane SM, Sohi MK, Wan T, Payne DJ, Bateson JH, Mitchell T, Sutton BJ (1998) Biochemistry 37:12404–12411
18. Carfi A, Duee E, Galleni M, Frere JM, Dideberg O (1998) Acta Crystallogr Sect D 54:313–323
19. Yang Y, Keeney D, Tang X, Canfield N, Rasmussen BA (1999) J Biol Chem 274:15706–15711
20. Wang Z, Benkovic SJ (1998) J Biol Chem 273:22402–22408
21. McManus-Munoz S, Crowder MW (1999) Biochemistry 38:1547–1553
22. Spencer J, Clarke AR, Walsh TR (2001) J Biol Chem 276:33638–33644
23. Suarez D, Merz KM Jr (2001) J Am Chem Soc 123:3759–3770
24. Diaz N, Suarez D, Merz KM Jr (2001) J Am Chem Soc 123:9867–9879
25. Diaz N, Suárez D, Merz KMJ (2000) J Am Chem Soc 122:4197–4208
26. Rasia RM, Vila AJ (2002) Biochemistry 41:1853–1860

27. Chantalat L, Duee E, Galleni M, Frere JM, Dideberg O (2000) Protein Sci 9:1402–1406
28. Carloni P, Blochl P, Parrinello M (1995) J Phys Chem 99:1338–1348
29. Car R, Parrinello M (1985) Phys Rev Lett 55:2471–2474
30. Hutter J, Alavi A, Deutsch T, Silvestri W, Parrinello M (2000) CPMD. MPI fur Festkorperforschung/IBM Research, Stuttgart/Zurich
31. Becke AD (1988) Phys Rev A 38:3098–3100
32. Lee C, Yang W, Parr RG (1988) Phys Rev B 37:785–789
33. Carloni P, Röthlisberger U (2000) In: Eriksson L (ed) Theoretical biochemistry – processes and properties of biological systems. Elsevier, Amsterdam, pp 215–252
34. Troullier N, Martins JL (1991) Phys Rev B 43:1943–2006
35. Kleinman L, Bylander DM (1982) Phys Rev Lett 48:1425–1431
36. Röthlisberger U (1998) ACS Symp Ser 712:264–273
37. Gervasio FL, Schettino V, Mangani S, Krack M, Carloni P, Parrinello M (2002) J Am Chem Soc (in press)
38. Martyna GJ, Tuckerman ME (1999) J Chem Phys 110:2810–2815
39. Hutter J, Luthi HP, Parrinello M (1994) Comput Mater Sci 2:244–248
40. Jiang J, Wang Y, Chang H, Lin SH, Lee YT, Niedner-Schatteburg G, Chang H (2000) J Am Chem Soc 122:1398–1410
41. Cox SR, Kollman PA (1984) J Comput Chem 5:129–136
42. Boys SF (1960) Rev Mod Phys 32:296–307
43. Marzari N, Vanderbilt D (1997) Phys Rev B 56:12847–12865
44. Piana S, Sebastiani D, Carloni P, Parrinello M (2001) J Am Chem Soc 123:8730–8737
45. Carfi A, Pares S, Duee E, Galleni M, Duez C, Frere JM, Dideberg O (1995) EMBO J 14:4914–4921
46. Lim HM, Iyer RK, Pene JJ (1991) Biochem J 276:401–404
47. Merz KM Jr (1990) J Mol Biol 214:799–802